Int J Earth Sci (Geol Rundsch) (2004) 93:596–611
DOI 10.1007/s00531-004-0402-y

ORIGINAL PAPER

Xiqiu Han · Erwin Suess · Heiko Sahling · Klaus Wallmann

Fluid venting activity on the Costa Rica margin: new results from authigenic carbonates

Received: 7 February 2004 / Accepted: 27 May 2004 / Published online: 14 August 2004

Abstract Carbonate precipitates on mounds and along tectonic scarps off the Costa Rica margin are manifestations of subduction-induced dewatering. The long-term dewatering history is recorded in mineralogical, petrological and isotope signals of carbonates recovered from these sites. The carbonates are strongly depleted in $\delta^{13}C$ (−11 to −53‰ PDB) and enriched in $\delta^{18}O$ (+4 to +8‰ PDB). Thermogenic methane and biogenic methane were identified as sources of the carbon. Chemoherm carbonates and seepage-associated carbonates formed in a focused flow regime have lighter $\delta^{13}C$ values, while others formed in a more diffusive flow regime have slightly enriched C isotope values. Three fluid components were inferred based on the calculation of equilibrium $\delta^{18}O$: clay dehydration water, gas hydrate water and seawater. Calculated equilibrium $\delta^{18}O$ values of carbonates from different down-core depths as well as from different precipitation stages show that the $\delta^{18}O$ of the precipitating fluid is progressively depleted with time. Dolostones showing a methane-C source and a well constrained O-isotope signature are thought to have formed at depth in the sediment and subsequently became exhumed. Glauconitic sandstones cemented by methane-derived carbonate provide evidence that fluid and solid material have been expelled by the mud volcano.

X. Han (✉) · E. Suess · H. Sahling · K. Wallmann
Sonderforschungsbereich 574 and GEOMAR,
Research Center for Marine Geosciences,
Wischhofstrasse 1–3, 24148 Kiel, Germany
e-mail: xiqiuhan@hotmail.com

X. Han
Key Laboratory of Submarine Geosciences & Second Institute of Oceanography,
State Oceanic Administration,
310012 Hangzhou, Zhejiang, China

Present address:
H. Sahling, Research Center for Ocean Margins,
University of Bremen,
Postfach 330440, 28334 Bremen, Germany

Keywords Authigenic carbonates · C- and O- isotopes · Petrology · Fluid venting · Costa Rica margin

Introduction

Authigenic carbonates at cold vent sites are associated with dewatering at active and passive continental margins worldwide (Suess et al. 1985; Kulm et al. 1986; Bohrmann et al. 1998; Greinert et al. 2001; Peckmann et al. 2001). The precipitation of these carbonates is driven by the anaerobic oxidation of methane (AOM) via a microbial consortium capable of simultaneously reducing sulfate and oxidizing methane (Boetius et al. 2000; Suess 2002a, 2002b). Mud mounds as well as slump scarps and faults covered with an impenetrable cap of such authigenic carbonates were discovered and sampled along the Middle American subduction zone off Costa Rica and Nicaragua during expeditions 144 and 163 of RV SONNE (Bohrmann et al. 2002a; Weinrebe and Flüh 2000). A supplemental collection of carbonates was taken from these mud extrusion and slump features during cruises of RV METEOR (M54/2- and -3) in 2002.

From the geologic setting of the Middle American subduction zone it is expected and has been recently shown that deeply sourced fluids from the overriding as well as the subducting plates are advected upward and expelled at the seafloor (Hensen et al. 2004). Since it is hardly feasible to monitor and determine the composition of the expelled fluids directly over long periods of time, collection and analysis of authigenic carbonates may provide an excellent archive of long-term fluid-venting history. Accordingly, we have used different approaches to characterize the nature, source and evolution of the fluid venting by examining the mineralogic, petrographic and isotopic characteristics of the carbonates. This includes tracking the C- and O-isotopes through reaction pathways involved in carbonate precipitation, identifying the methane-C source, i.e., whether it is deep thermogenic or shallow biogenic, and calculating the equilibrium ^{18}O-composition of the precipitating fluid. The latter approach

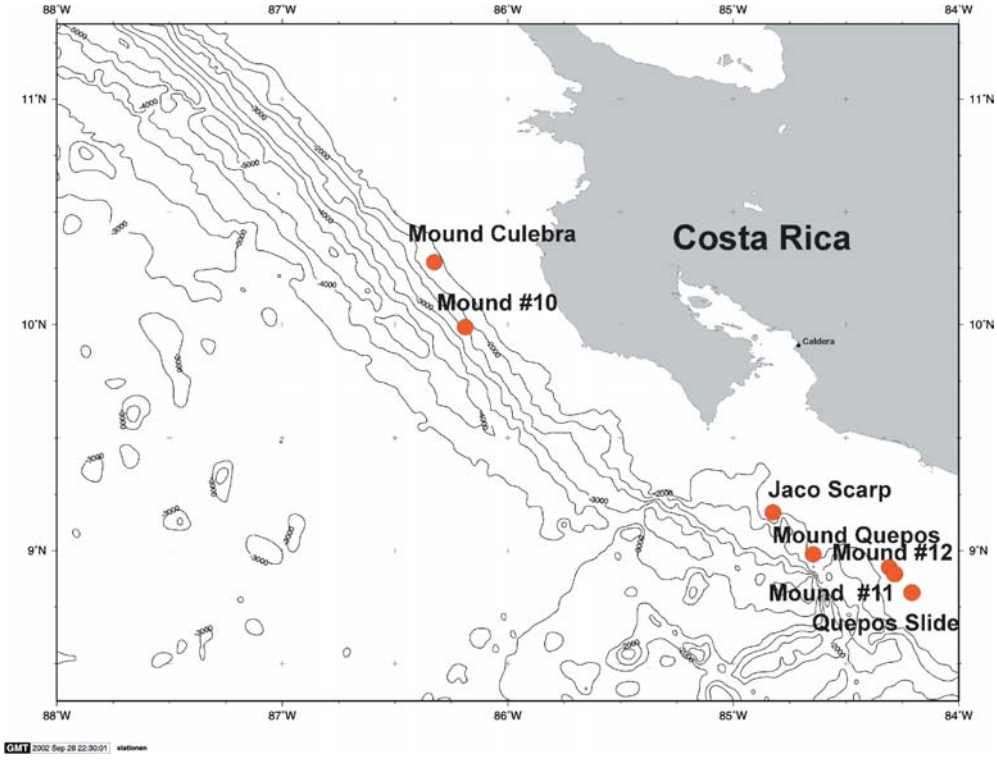

Fig. 1 Area of study and sites of sampling; numerous mounds, faults and slump features with extensive authigenic carbonates are concentrated along the mid-slope area in water depths between 800–1,500 m

is the opposite of that usually done in calculating the temperature of formation from the O-isotopes of carbonates.

Geologic setting and sampling sites

At the Middle American subduction zone, the Cocos Plate carrying a succession of hemipelagic and pelagic sediments subducts at a rate of about 88 mm/a underneath the Caribbean Plate (Hey 1977; Kimura et al. 1997). Tectonic erosion is the dominant process at the front and underside of the overriding plate, causing a progressive thinning of the margin and a well expressed system of extensional faults across the mid-slope off Costa Rica and Nicaragua (von Huene and Lallemand 1990; Le Pichon et al. 1993; Ranero and von Huene 2000; Vannuchi et al. 2001; Ranero et al. 2003; von Huene and Ranero 2003). Margin subsidence caused by removal of material from the base of the overriding plate is another consequence of tectonic erosion.

Compaction and dewatering causes a loss of 20–40% volume of the hemipelagic section of the underthrust oceanic sediments (Saito and Goldberg 2001). This significant volume of expelled water together with fluidized mud that may have its source at the plate boundary is channeled upwards and out onto the seafloor by deep faults. It is manifested as fluid-venting sites, usually in the form of mud mounds populated by vent communities and capped by authigenic carbonates. Another type of fluid escape features are slump scarps and slope failures. Prominent among these are those caused by seamounts or oceanic ridges riding on the subducted plate which plow into the sediments of the upper plate. This process disrupts strata either through upward bulging or slope collapse during and after passage of the seamount. The disrupted strata as well as the slump mass are also prime sites for fluid escape and associated authigenic carbonates.

The area of study and the sampling sites are shown in Fig. 1; numerous mounds, faults and slump features are concentrated along the mid-slope area in water depths between 800–1,500 m. More than 300 pieces of authigenic carbonates were collected from the mounds and slump features (Mound Culebra, Mounds #11, #12, Mound Quepos, Jaco Scarp, Quepos slide). Ocean floor observation (OFOS) revealed that the mounds and scarps are venting sites with a vigorous methane flux from below through a network of fault zones. Sediment cores taken at these sites provide ancillary information on pore water chemistry related to the formation of carbonates. TV-guided grabs (TVG), TV-guided multicores (TV-MUC) and gravity cores (GC) were used for sampling.

Methods

All of the rock specimens were examined and described morphologically, then representative samples were selected for further study. Based on macroscopic and microscopic fabric, subsamples were taken for mineralogic, isotopic and geochemical analyses to represent different stages of carbonate formation wherever possible. The mineralogy of the carbonates was determined by standard

powder X-ray diffraction analyses using a Philips PW 1820 diffractometer. XRD patterns were obtained from 3–70° 2θ at a low scan speed of 0.02° per second. The d [101] peak of quartz was used as internal standard. The MacDiff 4.2.5 program was used to separate overlapping peaks and to obtain the area of individual peaks of the carbonate mineral phases. The percentages of $MgCO_3$ in calcite were calculated from the d [104] shift using the average of the linear correlation of Goldsmith (1961) and Lumsden (1979). Calcite with less than 5 mol% $MgCO_3$ is considered low-Mg calcite (LMC), otherwise it is referred to as high-Mg calcite (HMC). The relative weight percentages of HMC, LMC, aragonite and (proto)-dolomite were calculated using the linear correlation by Milliman (1977).

Carbon- and oxygen-isotope ratios were measured on a Finnigan MAT 252 gas mass- spectrometer. The CO_2 extraction for $\delta\ ^{13}C$ and $\delta\ ^{18}O$ measurements was carried out with pure H_3PO_4 at 75 °C. The data are reported relative to the PDB standard. Replicate analyses of a laboratory standard show a standard deviation better than 0.03‰ for $\delta\ ^{13}C$ and 0.01‰ for $\delta\ ^{18}O$. The equilibrium isotopic compositions of the precipitating fluids for aragonite, HMC, LMC and proto-dolomite were calculated according to the fractionation equations of Grossman and Ku (1986), Friedman and O' Neil (1977), Kim and O'Neil (1997) and Irwin (1980), respectively, using the current temperatures of bottom water at the sampling sites and assuming, as a first approximation, that the pH of the precipitating fluid is that of seawater during carbonate formation. For those samples collected from and presumably formed in contact with bottom water, the assumptions about temperature and pH will certainly hold true. For those recovered and presumably formed at depth, an uncertainty remains. According to sediment temperature measurements and heat flow considerations in the area (Grevemeyer et al. 2004), an assumed ±0.5 °C uncertainty would imply formation within the uppermost 10 m of the sediment column. Since all buried samples were recovered from <10 m of depth, the assumed temperature of formation is probably correct. The uncertainty of 0.5 °C for formation temperature would correspond to only < ±0.13‰ PDB depending on different carbonate mineral phases.

Characteristics of authigenic carbonates at cold vents

Five types of authigenic carbonates were recognized by their morphology, mineralogy, petrology and C- and O-isotopic compositions. They are chemoherm carbonates, seepage-associated concretions, gas hydrate-associated concretions, and calcareous and dolomitic concretions. They are described below, and their distribution according to sampling sites, $MgCO_3$ content, and mineral composition are shown in Table 1.

Chemoherm carbonates

Chemoherms are free-standing edifices of carbonate in contact with bottom water. They have been defined as analogous to bioherms but with the emphasis that they are precipitates caused by chemosynthetic organisms living on cold vent sites (Aharon 1994; Bohrmann et al. 1998). The chemoherm carbonates offshore Costa Rica are such free-standing features containing shell debris from vent clams as well as clasts cemented by aragonite, all incorporated into a massive body of carbonate rock. Typical chemoherm carbonates were sampled from the Jaco Scarp plateau above the headwall and from Mound #12 (M54/TVG 172; SO163/TVG 4–4-1/-2) (Fig. 2A, B). At Jaco Scarp, the chemoherms grow on a dolostone hardground, contain abundant shell debris (*Bathymodiolus* fragments), and show at least two generations of aragonite layers lining void spaces. Below the aragonite layers the rock contains 85% carbonate of which 95% is aragonite and 5% high-Mg calcite (HMC; 11 mol% $MgCO_3$). At Mound #12 the samples were taken from the surface of the extended and fractured pavement that covers the summit. The fracture fillings are cemented by

Table 1 Lithology, $MgCO_3$ content and mineral composition of different types of authigenic carbonates from the Costa Rica margin

Location	Lithology	Mineral composition	$MgCO_3$ (mol%) in calcite		No. of samples
			Range	Average	
Mound Culebra	Tabular conglomerated concretion (type 4)	HMC, LMC	4–8	6	2
Mound #10	Massive & elongated concretion (type 4)	HMC, LMC	2–9	6	8
Mound #11	Gashydrate-associated concretion (type 3)	HMC, Aragonite, LMC	3–17	11	5
	Dolomitic concretion (type 5)	Dolomite	48	48	1
Mound #12	Seepage-associated concretion (type 2)	HMC	16–17	16.5	2
	Chemoherm (type 1)	Aragonite, HMC	16	16	1
	Bioturbation tube (type 4)	LMC	3	3	1
Mound Quepos	Seepage-associated concretion (type 2)	HMC	15	15	1
	Tubular concretion (type 4)	LMC, HMC	4–7	6	9
Quepos slide	Tabular micritic crust (type 2)	HMC	14	14	1
Jaco Scarp	Chemoherm (type 1)	Aragonite, HMC	11	11	1
	Dolomitic nodules & molds (type 5)	Protodolomite	40–49	47	6

Type 1: Chemoherm carbonates; Type 2: Seepage-associated concretions; Type 3: Gashydrate-associated concretions; Type 4: Calcareous concretions; Type 5: Dolomitic concretions

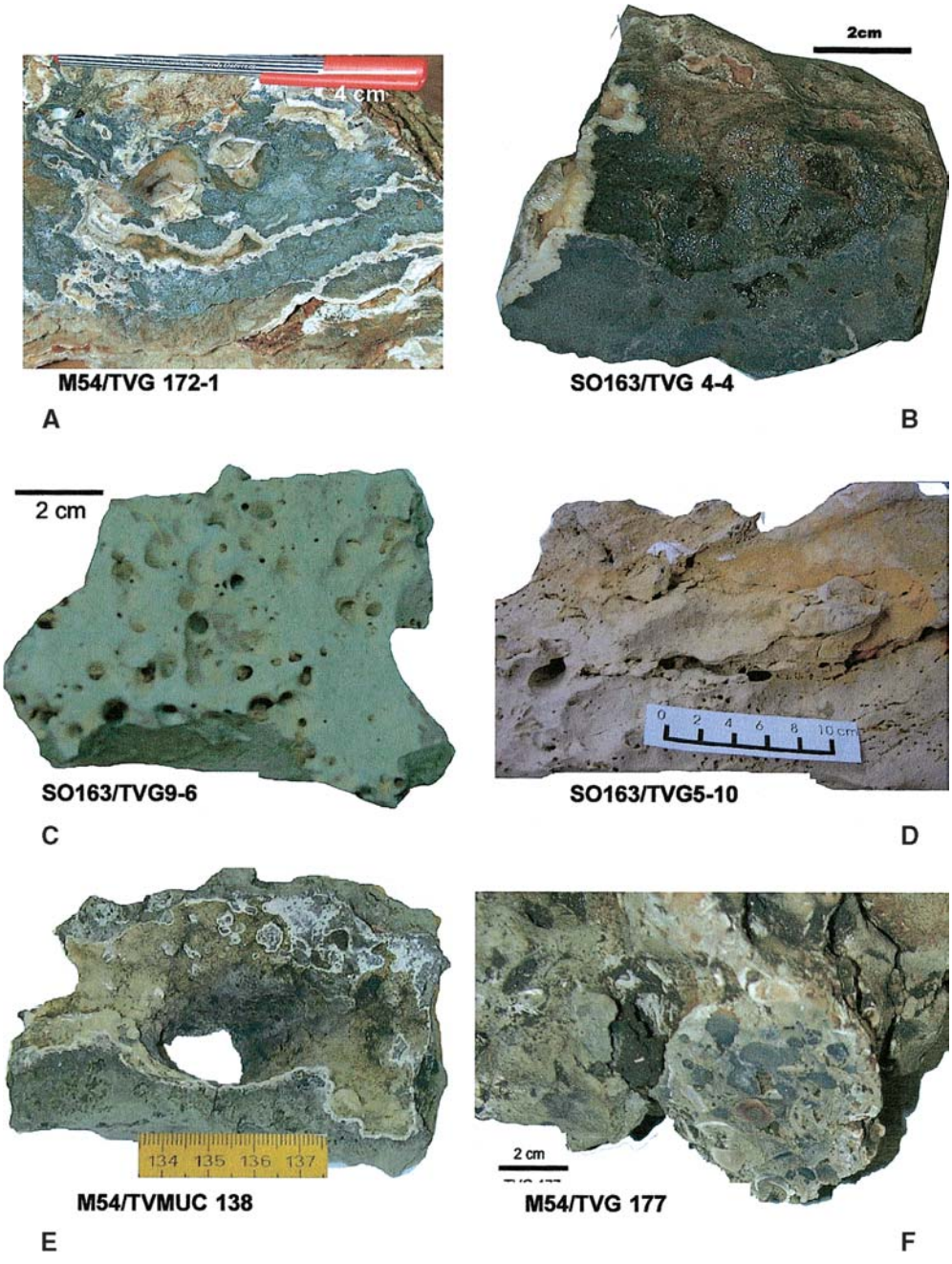

Fig. 2 Typical morphologies of chemoherm carbonates, seepage-associated crusts and gas hydrate-associated carbonates. **A** Chemoherm carbonate; abundant shell debris (*Bathymodiolus* fragments) and cemented clasts, aragonite layers lining free void spaces; Jaco Scarp, M54/TVG172. **B** Chemoherm carbonate; aragonite cemented sandstone breccia and shell debris, Mound #12, SO163/TVG4–4. **C** Seepage-associated crust; abundant mm-sized sinuous voids (2–5 mm diameter, associated with juvenile pogonophorans), Mound Quepos, SO163/TVG9–6. **D** Seepage-associated crust; cm-sized tubular voids associated with juvenile pogonophorans and arranged in direction of focused flow, Mound #12, SO163/TVG5–10. **E** Gas hydrate associated carbonate; micritic funnel-shaped chimney (*narrow opening upward*), with light-colored aragonite lining, Mound #11, M54/TVMUC138. **F** Gas hydrate associated carbonate; high-Mg-calcite (HMC)-cemented breccia of clay clasts and shell fragments, probably formed by break-up of gas hydrate layers, Mound #11, M54/TVG177

aragonite which also fringes every available void space. The matrix is composed of calcareous sandstone clasts and shell debris, containing 55% carbonate of which 81% is HMC (16 mol% $MgCO_3$) and 19% is aragonite. Thin sections show that sandstone is composed of quartz, glauconite and clay clasts subjected to some degree of diagenesis; for example, quartz grains partly replaced by calcite. Accordingly, the rock at Mound #12 contains two generations of carbonate cementation; here the HMC-cemented sandstone appears to be material of deep origin which had been uplifted and fractured. Fracturing provided the pathways for subsequent fluid escape and methane supply to the chemosynthetic communities, resulting in aragonite precipitation. At some places on Mound #12 the aragonite precipitates form edifices standing above the HMC-cemented sandstone pavement.

Type 2: Seepage-associated concretions

This type of carbonate concretion is similar to chemoherm carbonate in that it occurs at or near the seafloor in association with abundant vent communities. It differs from chemoherms in not forming free-standing edifices but rather small, individual carbonate blocks, concretions and crusts, usually with abundant mm- to cm-sized voids. Typical seepage-associated samples were found at Mound Quepos (SO163/TVG 9–6, Fig. 2C) and Mound

#12 (SO163/TVG 5-10, Fig. 2D), with concretions a few cm thick containing voids (Fig. 2C) and channels (Fig. 2D). Most voids were inhabited by juvenile vestimentiferan tubeworms (*Lamellibrachia barhami*). The interaction between the carbonates and the tubeworms is unknown, but we speculate that carbonate and tubeworm grow concomitantly, creating the voids and channels. Carbonates precipitate around living tubeworms where small newly-settled tubeworms may actively dissolve the carbonate or somehow keep the channels open so that fluids flow through abandoned voids. This type of carbonate is composed of HMC with $MgCO_3$ content in the range of 15–17 mol% and has a micritic texture (Table 1). Microcrystalline HMC and granular pyrites inside the voids and along the channels indicate that methane-charged fluid which flowed through the channels were oxidized in the presence of seawater sulfate and thus precipitated HMC and pyrite.

Type 3: Gas hydrate-associated concretions

Gas hydrate carbonates are a newly defined type of authigenic lithology related to methane oxidation where methane comes from dissociating gas hydrates and the precipitating fluid may contain some gas hydrate water (Bohrmann et al. 1998). They are characterized by layered aragonite growing into an open void space presumably left by dissociated gas hydrate. Occasionally, imprints of the hydrate texture, and brecciated fabric caused by collapse of void space, were observed in gas hydrate-associated carbonates (Suess et al. 2002; Bohrmann et al. 2002b). Such lithologies were recovered from Mound #11 where massive gas hydrate was also found approximately 200 cmbsf (cm below seafloor) (Soeding et al. 2003). The lithologies were a chimney-like concretion with aragonite lining (M54/TVMUC 138, Fig. 2E), an aragonite-cemented conglomerate containing mud breccia and shell fragments (M54/TVG 177, Fig. 2F), and at 111 cmbf at station M54/143 a glauconitic sandstone slab cemented by and sandwiched between aragonite layers (Fig. 3A). Sample M54/TVMUC 138 contains 70% carbonate, composed of 89% HMC (11 mol% $MgCO_3$) and 11% aragonite. Sample M54/TVG 177 contains 61% carbonate, composed of 8% LMC, 14% HMC and 78% aragonite. Sample M54/GC143–111 is composed of 70–80% detrital fraction and 20–30% aragonite and calcite (3–17 mol% $MgCO_3$) cement. The detrital fraction consists of glauconite (~60%), quartz (~30%), feldspar (~5%) and quartzite clasts (~5%). Most of the quartz crystals are angular and some are replaced by microcrystalline calcite along the edges (Fig. 4C). The surface of the glauconite appears "dirty" from granular pyrite precipitates. The host sediment of the sandstone slab contained abundant shell fragments with a big void (110–126 cmbsf) filled with water and surrounded by soft sandy sediments just below the slab. In situ, this void was probably filled with gas hydrate which disappeared when the core was retrieved and exposed to normal pressure and temperatures. The sediments below the void appeared dry as if dewatered by gas hydrate formation.

Type 4: Calcareous concretions

The calcareous concretions are interpreted as a result of anaerobic oxidation of methane- charged fluid. They are of tubular, irregular or massive shapes and are composed of LMC or HMC, but with relatively low $MgCO_3$ contents compared to those of seepage-associated concretions (Table 1). Typical tubular concretions are found at Mound Quepos, consisting of 1–4 individual conduits about 1 cm in diameter and tens of centimeters long. Adult specimens of the vestimentiferan tubeworm *Lamellibrachia barhami* were observed in some of these conduits, others were empty or had been filled in (Fig. 3C). Their walls were usually a few millimeters thick and composed of lithified sediments (Fig. 4D); the fillings sometimes including exotic and coarse-grained lithic material. Some of the conduits were completely filled in, but the outline of the original conduits could still be discerned from in cross sections. The mineral compositions of the walls are calcite with 4–7 mol% $MgCO_3$ (Table 1). The fillings had less $MgCO_3$ than the walls and also contained glauconite, quartz grains and angular clay clasts. The glauconite grains appeared altered, some of them fractured; others showed dissolution features or were replaced by quartz (Fig. 4E), indicating that the material might be relatively old and channeled upward from deeper strata. Mound #12 yielded abundant irregular concretions with sinuous conduits. The conduits were usually about 1 cm in diameter and less than 10 cm in length. Massive concretions, with a usually smooth surface and dense texture, were found at various depths in cores as well as on the surface of Mound #10 (Fig. 3D). There were four depth levels of concretions found downcore at Mound #10 (M54/GC133:28 cmbsf, 180 cmbsf, 279 cmbsf and 312 cmbsf). The concretions were dominated by LMC or HMC ($MgCO_3$<8 mol%) (Table 1), further decreasing in Mg-content with depth. The bulk of a concretion from the surface of Mound #10 contained 8 mol% $MgCO_3$ whereas a HMC vein was transformed into LMC suggesting that the concretion was not newly formed but were subjected to diagenesis (M54/GC133, Figs. 3D, 4F).

Type 5: Dolomitic concretions

Large round dolomitic nodules (tens of cm in diameter) and irregular dolomitic molds of burrows or fluid channels were found on the plateau above Jaco Scarp (Fig. 3E, F). They were composed of proto-dolomite, with micritic textures and containing 40–49 mol% $MgCO_3$ (Table 1). Several nodules have shrinking cracks in the center and dendritic pyrite growth along the micro-fissures in the outer layer (Fig. 3E). The dolostones probably formed well inside the sediment column but became exhumed when the strata were up-warped and eroded due to the

Fig. 3 Typical morphology of gas hydrate-associated carbonates, calcareous and dolomitic concretions. **A** Gas hydrate associated crust; HMC-cemented tabular glauconite sandstone and aragonite layers at 111cmbsf, Mound #11, M54/GC143–111. **B** Dolomitic concretion at 97 cmbsf; Mound #11, M54/GC143–97. **C** Calcareous concretion; micritic, tubular conduits about 1 cm in diameter, associated with adult pogonophorans partially filled with cemented sediments, Mound Quepos, SO163/TVG9–5. **D** Calcareous concretion; massive with dissolution features, Mound #10, M54/TVG 134–4. **E** Dolostone; dolomitic nodule with shrinking cracks, Jaco Scarp, SO163/TVG7–2. **F** Dolostone, concretion with mould of channel or burrows, brownish surface in contact with bottom water, Jaco Scarp SO163/TVG3–7

passage of the seamount underneath. TV-sled observations revealed dolomitic nodules and doughnut-shaped carbonates along faults with or without evidence of recent methane seepage. Similar rounded dolomitic carbonates were observed at Mound #11. Several lines of evidence indicate that erosion or flank collapse has removed the main part of the mound and exposed the ancient plumbing system as well as the recent central extrusion pathway (Mörz et al. 2004). Down-core at Mound #11 no large dolomitic carbonates were recovered but instead a small massive angular micritic dolostone was found at 97 cmbsf (M54/GC143 97, Fig. 3B). It is composed of proto-dolomite with 48 mol% $MgCO_3$, has a micritic texture with local recrystallization, and contains pyrite aggregates.

Carbon and oxygen isotope compositions

The results of stable isotope analyses are listed in Table 2 and shown in Fig. 5. All of the samples are depleted in ^{13}C and enriched in ^{18}O over seawater. Chemoherm carbonates and seepage-associated crusts are characterized by carbon isotope ratios ranging from −46 to −53‰ PDB, having the most extreme ^{13}C-depletion. The gas hydrate-

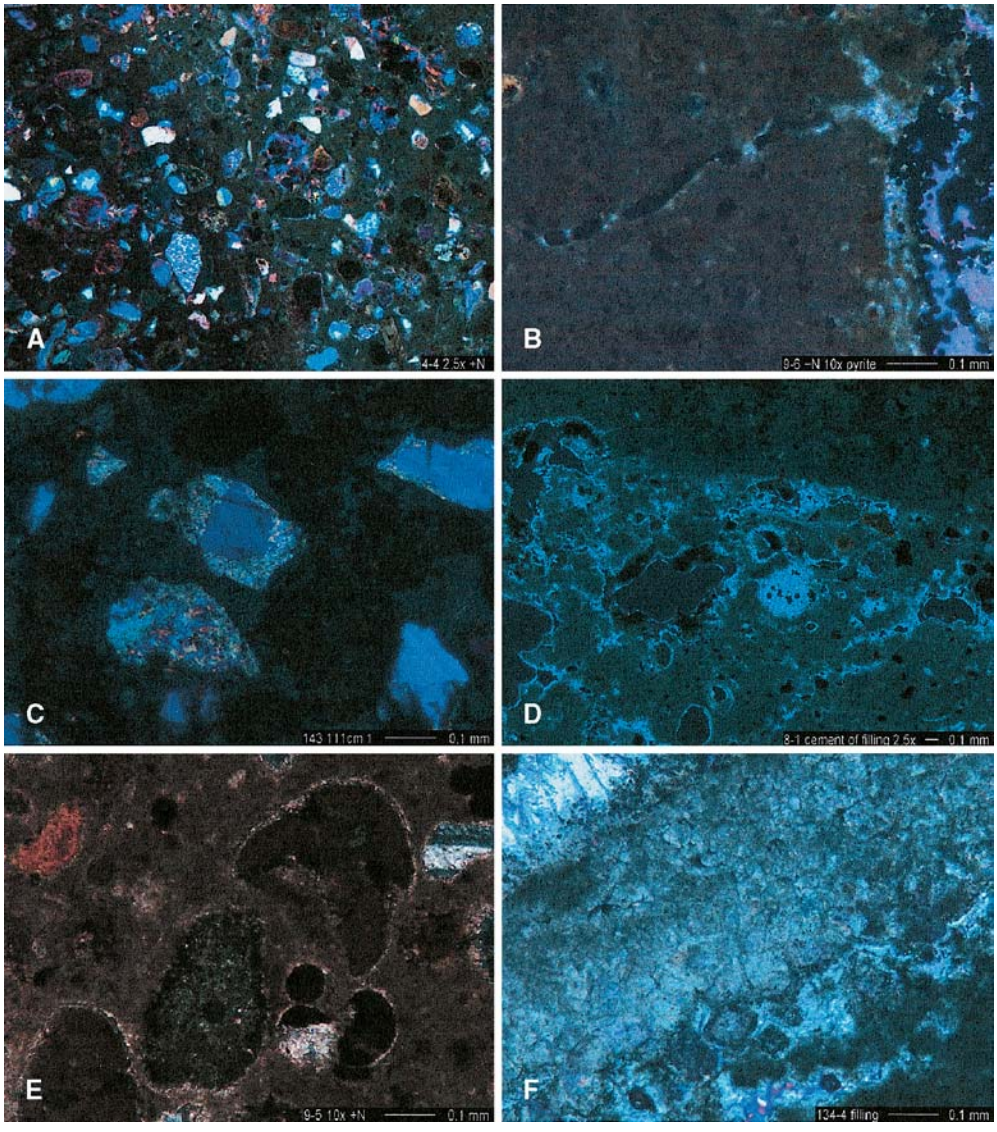

Fig 4 Thin-section photomicrographs of authigenic carbonates in crossed-polarized light. **A** Calcareous glauconite sandstone, matrix support, glauconite diagenetically altered; subrounded quartz partially replaced by calcite, Mound #12 SO163/TVG4–4. **B** Pyrite, black globular formations in voids and fluid channels in seepage associated crust; Mound Quepos, SO163/TVG9–6. **C** Calcareous glauconite sandstone, quartz partially replaced by calcite, pyrite on surface of glauconite grains, M54/GC143–111. **D** Tubular calcareous concretion showing different fabrics of wall (*upper right part*) and filling (*lower left part*), Mound Quepos, SO163/TVG8–1. **E** Fabric of filling of tubular calcareous concretion composed of glauconite, quartz and clay clasts, Mound Quepos, SO163/TVG9–5. **F** High Mg-calcite (*HMC*) vein, partially transformed into low-Mg-calcite (*rhombs at center bottom*), Mound #10, M54/TVG134–4

associated concretions, however, have enriched carbon isotope ratios in the range of −19 to −30‰ PDB. The calcareous concretions (−32 to −49‰ PDB) are intermediate between these two groups. The carbon isotopes of the dolomitic concretions scatter widely between −11 and −44‰ PDB. The depleted carbon isotope values indicate that all carbonates are to some extent methane-derived, but the range of values indicates different methane-C sources. The oxygen isotope values range from +4.4 to +8.1‰ PDB, generally indicating an ^{18}O-enriched fluid source. Dolomitic concretions have relatively enriched oxygen isotope values (+5.7 to +8.1‰ PDB), while the chemoherm carbonates and seepage-associated crusts have relatively depleted values (+4.3 to +5.4‰ PDB); all other carbonate types have intermediate values. The isotope data for carbon and oxygen agree well with values typical for cold vent carbonates in other regions (Ritger et al. 1987; Kulm and Suess 1990; Paull et al. 1992; Roberts and Aharon 1994; Bohrmann et al. 1998; Greinert et al. 2001). This confirms that they formed as a result of anaerobic microbiological oxidation of methane supplied as a fluid component from below.

Discussion

Petrological, mineralogical and isotope geochemical data on the authigenic carbonates provide important clues for understanding their origin and formation mechanisms as well as the nature, source and flow patterns of venting fluids. A more detailed interpretation of the authigenic carbonate archives in terms of methane sources and types of precipitating fluid-as proposed here is based on pore water and methane data from the sampled sites, and on modeling results of the dynamics of fluid advection and carbonate precipitation at cold vent sites (Luff and Wallmann 2003; Hensen et al. 2004). Clarification of the reaction pathways of AOM and coupled carbonate formation within the sulfate reduction zone, determines that precipitation essentially occurs close to or at the sedi-

Table 2 C- and O-isotope characteristics of authigenic carbonates from the Costa Rica margin

Sample ID	Sample description	Sub-sampling position	$\delta^{13}C$ ‰ PDB	$\delta^{18}O$ ‰ PDB	Location
SO163/TVG2–2-1	Tabular conglomeration (Type 4)	Matrix	−33.7	6.3	Culebra
SO163/TVG2–2-2	Tabular conglomeration (Type 4)	Cement	−32.0	5.2	Culebra
M54/TVG172–1-1	Chemoherm (Type 1)	Aragonite cement	−46.0	5.0	Jaco Scarp
M54/TVG172–1-3	Chemoherm (Type 1)	Matrix	−51.0	4.8	Jaco Scarp
M54/TVG172–1-4	Dolostone (Type 5)	Inside	−30.8	8.1	Jaco Scarp
SO163/TVG 3–5-3	Dolomitic concretion (Type 5)	Inside	−29.0	6.8	Jaco Scarp
SO163/TVG3–9-2	Dolomitic concretion (Type 5),	Outside	−28.3	6.5	Jaco Scarp
SO163/TVG7–1-1	Half-buried dolomitic nodule (Type 5)	Outside	−44.2	5.7	Jaco Scarp
SO163/TVG7–1-2	Half-buried dolomitic nodule (Type 5)	Inside	−31.6	7.0	Jaco Scarp
SO163/TVG7–2	Pale-green dolomitic nodule (Type 5)	Inside	−40.5	8.0	Jaco Scarp
M54/GC133–279	Calcareous concretion, 279–280 cmbsf (Type 4)	Matrix	−44.1	5.8	Mound #10
M54/GC133–312	Calcareous concretion, 312–315 cmbsf (Type 4)	Matrix	−39.0	5.6	Mound #10
M54/GC133–180	Calcareous concretion, 180–185 cmbsf (Type 4)	Matrix	−44.6	5.5	Mound #10
M54/GC133–28	Calcareous concretion, 28–32 cmbsf (Type 4)	Matrix	−42.4	5.4	Mound #10
M54/TVG134–2-2	Tabular micritic breccia (Type 4)	Matrix	−53.0	5.4	Mound #10
M54/TVG134–3-2	Massive limestone with smooth surface (Type 4)	Matrix	−44.3	6.7	Mound #10
M54/TVG134–4-1	Massive limestone with smooth surface (Type 4)	HMC vein	−27.4	6.3	Mound #10
M54/TVG134–6-2	Burrow concretion (Type 4)	Matrix	−48.5	6.0	Mound #10
M54/ TVMUC138–1	Gashydrate-associated concretion (Type 3)	Aragonite layer	−22.7	5.1	Mound #11
M54/ TVMUC138–2	Gashydrate-associated concretion (Type 3)	Matrix	−18.6	6.0	Mound #10
M54/GC143–97	Massive dolostone (Type 5), 97cmbsf	Inside	−11.1	6.4	Mound #10
M54/GC143–111 A	Gashydrate-associated concretion (Type 3)	Upper side	−29.4	5.4	Mound #10
M54/GC143–111 C	Gashydrate-associated crust (Type 3)	Down side	−29.8	6.8	Mound #10
M54/TVG177	Gashydrated-associated breccia (Type 3)	Matrix	−22.0	5.2	Mound #10
SO163/TVG4–4-1	Chemoherm (Type 1)	Arogonite cement	−49.2	4.4	Mound #12
SO163/TVG4–4-2	Chemoherm (Type 4)	Clast	−40.6	6.4	Mound #12
SO163/TVG5–1	Bioturbation tube (Type 4)	Wall	−30.2	6.8	Mound #12
SO163/TVG5–8-1	Lithified sediments (Type 2)	Cement	−49.9	5.4	Mound #12
SO163/TVG5–8-2	Lithified sediments (Type 2)	Matrix	−50.9	4.3	Mound #12
SO163/TVG8–1	Tubular concretion (Type 4)	Filling	−37.2	6.2	Mound Quepos
SO163/TVG8–1-2	Tubular concretion (Type 4)	Wall	−38.3	5.8	Mound Quepos
SO163/TVG8–2-1	Tubular concretion (Type 4)	Inside	−37.5	6.0	Mound Quepos
SO163/TVG9–2-1	Tubular concretion (Type 4)	Inside	−40.4	6.0	Mound Quepos
SO163/TVG9–2-2	Tubular concretion (Type 4)	Inside	−32.4	6.4	Mound Quepos
SO163/TVG9–2-3	Tubular concretion (Type 4)	Outside	−41.5	6.0	Mound Quepos
SO163/TVG9–3-1	Tubular concretion (Type 4)	Inside	−37.5	5.8	Mound Quepos
SO163/TVG9–5-1	Tubular concretion (Type 4)	Filling	−34.2	6.0	Mound Quepos
SO163/TVG9–5-2	Tubular concretion (Type 4)	Matrix	−32.7	5.8	Mound Quepos
SO163/TVG9–6	Tabular micrite crust with cm sized voids (Type 2)	Matrix	−52.7	4.8	Mound Quepos
SO163/TVG6–3-2	Tabular micrite crust (Type 2)	Matrix	−51.9	4.9	Quepos slide

Note: Type 1: Chemoherm carbonates; Type 2: Seepage-associated carbonates; Type 3: Gashydrate-associated carbonates; Type 4: Calcareous concretions; Type 5: Dolomitic concretions

ment/water interface. This is an important constraint because it establishes that temperature of formation is the same as that of bottom water and that the pH is predictable to within ±0.1 pH unit. Both parameters, if known, allow calculation of the equilibrium O-isotope composition of the precipitating fluid. These calculated data reveal important information on the source depth and origin of advecting fluids.

Precipitation reactions and isotope tracking

Methane, either from gas hydrates or as dissolved or free gas advecting upwards at cold vent sites, greatly stimulates microbial activity at the seafloor and over a finite sediment thickness near the seafloor. The base of this zone is known as the sulfate-methane-interface (SMI), which varies in depth below sea floor depending on the relative rates of methane supply from below and sulfate from above (Borowski et al. 1999; Luff and Wallmann 2003). Accordingly, several scenarios of authigenic carbonate formation may develop: those in contact with free bottom water, those in contact with pore water within a narrow layer of AOM, and those forming within a thicker AOM-layer. Additionally, the mode of methane supply as free gas bubbles, dissolved in the ascending fluid, or dissociating from gas hydrate may also affect the carbonate characteristics.

The biogeochemical process underlying carbonate formation and its intimate association with methane and gas hydrate can be seen from the reactions shown in Table 3 (modified from Suess 2002a, 2002b). Gas hydrates or free and dissolved gas provide an almost inexhaustible supply of isotopically “light” methane from biogenic as well as thermogenic sources which is transformed by the microbial consortium into bicarbonate. This bicarbonate equi-

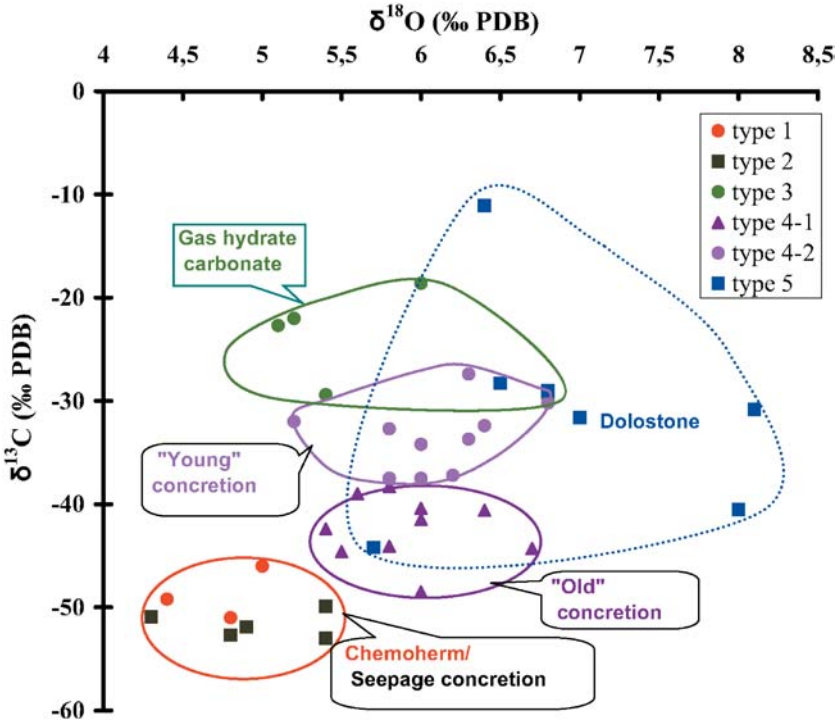

Fig 5 Carbon and oxygen isotope composition of all authigenic carbonates obtained from study area; grouping is based on isotopic, petrographic, mineralogic and morphological criteria which are explained in the text; type *1* = chemoherm and type *2* = seepage associated carbonates; type *3* = gas hydrate-associated carbonates; type *5* = dolomitic concretions, calcareous concretions divided into "early"-stage (type *4–1*) and "late"-stage (type *4–2*) precipitates

Table 3 Reactions and progression of stable C- and O-isotope signatures during methane oxidation by microbial consortia leading to authigenic carbonate mineral formation; basically, methane-C and altered water-O propagate through a series of equilibrium reactions and are incorporated into authigenic carbonate phases

Oxidation of methane from gas hydrate, thermogenic or biogenic sources
$CH_4 + SO_4^{2-} \rightarrow HCO_3^- + HS^- + H_2O$
Oxygen isotopes are exchanged between the dissolved inorganic carbon pool and water derived from hydrate dissociation, clay dehydration or seawater
$H_2O + CO_2 \leftrightarrow HCO_3^- + H^+$
Carbonate equilibrium
$HCO_3^- \leftrightarrow H^+ + CO_3^{2-}$
Precipitation of carbonate mineral phases
$CO_3^{2-} + Ca^{2+} \leftrightarrow CaCO_3$
Sulfide removal: Oxidation by microbial communities
$HS^- + 8/5\ NO_3^- + 3/5\ H^+ \rightarrow SO_4^{2-} + 4/5\ N_2 + 4/5\ H_2O$
$HS^- + 2\ O_2 \leftrightarrow SO_4^{2-} + H^+$
Sulfide removal: Fe-sulfide formation
$HS^- + Fe^{2+} \leftrightarrow FeS + H^+$
Sulfide removal: Ebullition (bubble stripping)
$H^+ + HS^- \leftrightarrow H_2S$

librates with pore water containing a ^{18}O-composition with an ^{18}O-signal characteristic of either hydrate water, clay dehydration water or ancient seawater. The different fluids involved in carbonate formation carry a distinct oxygen isotope signal "heavier" than that expected from normal seawater. This "heavy" oxygen isotope signal is recorded by the precipitating $CaCO_3$-phases along with the isotopically "light" methane-carbon. For precipitation to proceed and continue to build up carbonates, the hydrogen sulfide generated by methane oxidation via sulfate reduction must be continuously removed from the system. Since removal may take several reactions (Table 3 bottom), only ebullition (bubble stripping) and oxidation via nitrate directly promote carbonate precipitation, whereas Fe-sulfide precipitation and oxidation via free oxygen cause carbonate dissolution. The removal of sulfide by nitrate and oxygen is chemoautotrophically achieved by another community, usually consisting of *Beggiatoa* mats or microbes living in bivalves and tube worms found in close proximity to the AOM-consortia. The presence of pyrite in carbonates suggests that both competing reactions occur (Figs. 2C, 4B), but carbonate precipitation is by far dominant.

End-member carbon sources and oxygen isotope signature

Stable carbon and oxygen isotope data identify four subgroups of methane-derived carbonates from several different vent sites and different fluid-source zones. The seepage associated crusts and chemoherm carbonates have the most depleted C isotope signature, while the gas-hydrate associated carbonates are enriched in C isotope.

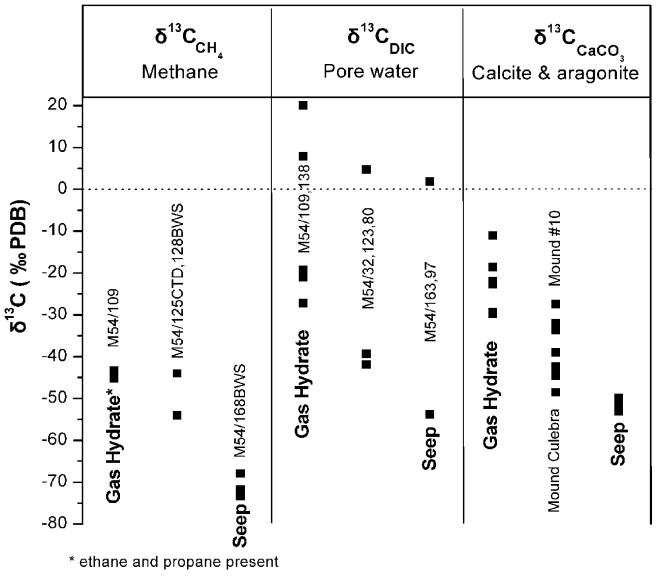

Fig 6 C-isotope composition of different end-member methane pools. *Left column*: Water column methane: δ^{13}C of thermogenic deep methane from gas hydrate, Mound #11 (M54/109); from biogenic methane seep, Mound #12 (M54/168BWS), Mound Culebra (M54/128BWS) and Mound #10 (M54/125CTD). *Middle column*: Dissolved inorganic carbon (DIC) in pore water: δ ^{13}C of DIC from Mound #11 (M54/109 and M54/138), from seep cores in Mound #12 (M54/163,97), and from cores at Mound #10, M54/32,123, 80). *Right column*: Authigenic carbonates: δ ^{13}C of calcite or/and of aragonite from the same locations where water column methane and pore water DIC data were obtained

Their average difference is approximately 26‰ PDB. The same difference has been recorded in bottom water methane at the vent sites at the respective sites (Fig. 6): e.g. M54/168BWS from Mound #12 is about 30‰ PDB lighter than M54/109 from Mound #11. Furthermore, the gas from Mound #11 contained traces of ethane and propane, which together with the enriched C-isotopes is a clear indication of a deep thermogenic source. Thus the carbonates originate from the oxidation of two distinct pools: thermogenic methane from deep fluids and biogenic methane from shallow fluids. Additionally, as shown in Fig. 6, the pore waters from Mound #11 have a C-isotope ratio of dissolved inorganic carbon (DIC) of between +20 and −27‰ PDB for upward flow of deep fluids (M54/109, 138) and −54 to +1‰ PDB for upward flow of shallow fluids (M54/163, 97). These observations confirm two different types of methane-enriched fluids are being vented in the study area.

The first type of fluid ascends from the subducting slab to the surface through faults acting as high permeability conduits for focused flow. These deep fluids are released from clay minerals during smectite/illite transformation and other diagenetic processes at approximately 10 km below the surface and at temperatures of about 80–130 °C (Hensen et al. 2004). They are depleted in chloride and isotopically enriched in ^{18}O, with high concentrations of dissolved thermogenic methane, and DIC highly enriched in ^{13}C from deep methanogenesis (Claypool and Kaplan 1974). In case gas hydrates are present, the ^{18}O-enrichment may be amplified by the addition of ^{18}O-enriched hydrate water (Suess et al. 1999). The second type has a more shallow origin indicated by the presence of biogenic rather than thermogenic methane and the absence of other deep-fluid criteria such as ^{13}C-enriched DIC or boron (Hensen et al. 2004). Both types of fluids are subjected to anaerobic methane oxidation (AOM) causing carbonate precipitation during ascent and venting to the seafloor. Subsurface mixing between methane and sulfate-bearing fluids followed by AOM is suggested by the co-occurrence of dissolved sulfate, sulfide and methane in millimolar concentrations (Table 4).

The δ^{13}C of dissolved inorganic carbon (DIC) is significantly different in both types of fluids. The deep fluid DIC is highly enriched in ^{13}C while the shallow fluid DIC is strongly depleted. The deep fluid transports ^{13}C-enriched DIC and ^{13}C-depleted CH_4 to the surface, both generated via methanogenesis at depth (Claypool and Kaplan 1974). In contrast, the DIC of the shallow fluids does not have isotopic signatures of methanogenesis. There the ^{13}C-enriched DIC possibly has been separated from the ^{13}C-depleted CH_4 at depth so that only the depleted CH_4 is transported to the surface. The most likely process responsible for this selective transport is the formation of free gas at depth and the subsequent ascent of methane bubbles through the sediment column. A seismic BSR throughout the study area clearly demonstrates the presence of free gas below the gas hydrate stability zone (Pecher et al. 2001). Surface observations and ODP drilling at other convergent margins (Hydrate Ridge, off Oregon; Suess et al. 1999; Torres et al. 2003) reveal that free gas can be transported through sediment layers over a vertical distance of more than 100 m so that ^{13}C-depleted CH_4 rises to the surface. Gas bubbles ascending into the region above the BSR may dissolve in pore fluids and form solid gas hydrates. A minor fraction escaping dissolution and precipitation may reach the surface (Fig. 7,

Table 4 Characteristics of two different types of methane-rich fluids venting in the study area from which authigenic carbonates precipitate; data from Hensen et al. (2004)

	Deep fluids	Shallow fluids
Total alkalinity (mEquivalent per litre)	5 to 15	20–30 (25)
Total dissolved sulfide (mM)	0	5–15 (10)
Dissolved sulfate (mM)	0	1–5
Dissolved chloride (mM)	<200 to <500	555
Dissolved methane (mM)	70 gas saturation	20–70 (50)
δ^{18}O (‰ SMOW)	+5 to +3	+1 to −1 (0)
δ^{13}C of DIC (‰ PDB)	+8 to +20	−40 to −55 (−50)
δ^{13}C of CH_4 (‰ PDB)	−45 to −30	−70 to −80 (−75)

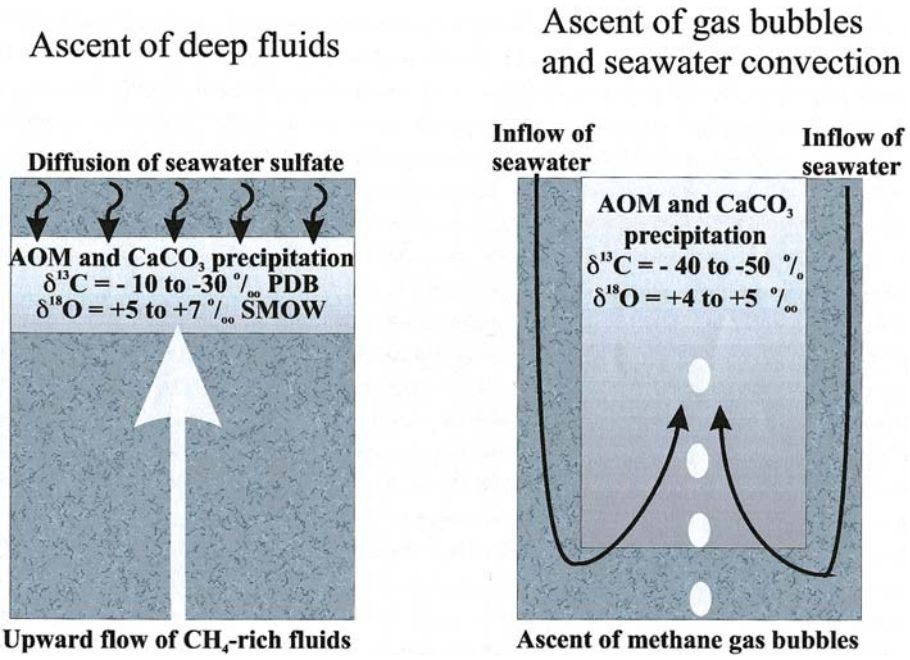

Fig. 7 Modes of carbonate formation and isotopic composition of venting-related carbonate minerals. *Left panel* shows formation of carbonates induced by the rapid ascent of deep fluids while *right panel* depicts carbonate precipitation caused by seawater convection and gas bubble ascent. Different isotopic composition of deep and shallow fluids (Table 3) and mixing processes induce marked contrast in isotopic composition of authigenic carbonates

right-hand panel) where persistent and vigorous gas ascent has been observed to induce convection of seawater through shallow surface sediments (O'Hara et al. 1995).

Pore water profiles show that the ascent of isotopically-altered deep fluids ($\delta^{18}O$ = +5‰ SMOW and $^{13}C_{DIC}$ = +8‰ PDB) is sometimes very rapid (up to 300 cm/year) and highly focused, so that little mixing occurs at depth (Hensen et al. 2004). In this case AOM and $CaCO_3$ precipitation are limited to a narrow zone close to the sediment surface where rising methane and downward diffusing seawater sulfate meet (Luff and Wallmann 2003). This situation, depicted in Fig. 7, generates a fluid with relatively enriched $\delta^{13}C$ (−10 to −30‰ PDB) and enriched $\delta^{18}O$ (+3 to +5‰ SMOW) values because of the presence of the isotopically enriched deep fluid and the admixture of depleted DIC generated by AOM ($\delta^{13}C$ = −40 to −50‰). The $\delta^{13}C$ of the precipitated carbonates is much lower than that of the corresponding methane because a large fraction of methane is not oxidized at these high flow rates, but is expelled into the overlying bottom water (Luff and Wallmann 2003). Many of the gas hydrate carbonates recovered from Mound #11 have a similar isotope signature suggesting that they were formed in a narrow precipitation zone close to the sediment surface by oxidation of thermogenic methane in rapidly ascending deep fluids.

Other carbonate samples have rather high $\delta^{18}O$ values implying the involvement of deep fluids. They are more depleted in ^{13}C ($\delta^{13}C$ = −30 to −40‰ PDB) than would be expected from ^{13}C of DIC (up to +20‰ PDB) and less depleted than the carbonates formed from free methane (^{13}C < −40‰ PDB). Such a signature could result when deep fluids ascend more slowly in a less focused mode, thus mixing with ambient pore fluids at depth and extensive methane oxidation in the shallow subsurface. Methane would then be oxidized using sulfate from the surrounding pore fluids as electron acceptor. As the deep fluids contain much more methane than DIC (Table 4), a complete oxidation of methane would generate fluids and carbonates with a $\delta^{13}C$ range reflecting mainly the isotopic composition of oxidized methane, although the mixing of small amounts of ^{13}C-enriched DIC would also generate ^{13}C-enriched carbonates. Many carbonate concretions have this signature implying that they were formed in the shallow subsurface by the mixing of slowly rising deep fluids with sulfate-bearing pore fluids.

Many chemoherm and seepage carbonates are strongly depleted in ^{13}C ($\delta^{13}C$ = −46 to −51‰) while their rather low $\delta^{18}O$ reflects equilibration with ambient bottom and pore waters. These carbonates are probably formed by the rapid ascent of shallow fluids containing biogenic methane with very negative $\delta^{13}C$ (−70 to −80‰) and isotopically depleted DIC generated by subsurface AOM (Table 3). The fluids may be formed by the ascent of gas bubbles inducing a convection of seawater through surface sediments (Fig. 7, left-hand panel). AOM zones and precipitation horizons thus are shifted to the surface by rapid upward fluid flow (Luff and Wallmann 2003) so that the depleted seepage and chemoherm carbonates either form close to the sediment surface or even grow into the water column. Some carbonate concretions showing evidence of having formed in deeper sediment horizons are also strongly depleted in ^{13}C. These were probably formed by the slow ascent of shallow fluids accompanied by subsurface mixing, AOM, and carbonate precipitation processes.

The equilibrium isotopic composition of the fluid

The oxygen isotopic composition of a carbonate depends on the formation temperature, the oxygen isotopic com-

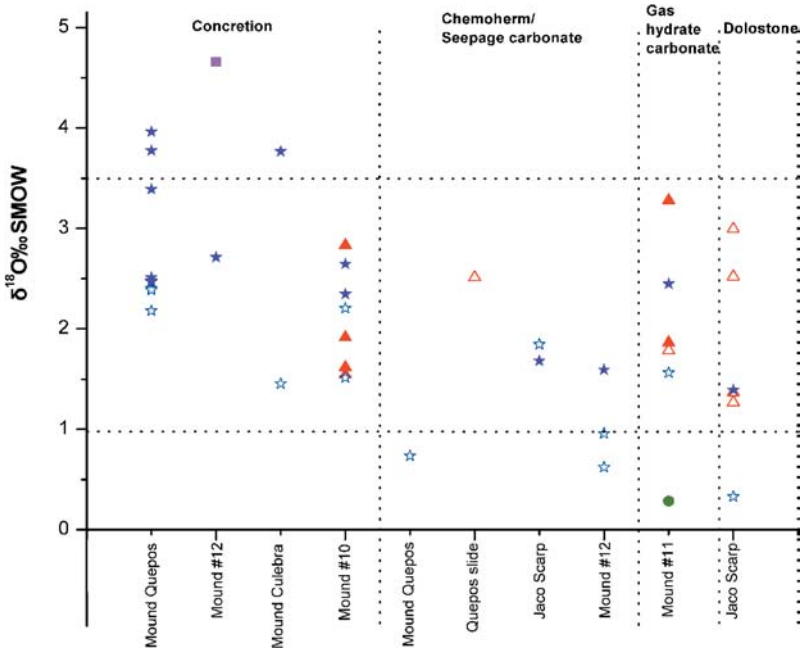

Fig. 8 Equilibrium composition of precipitating fluids calculated for various carbonate minerals at current bottom water temperature at sites of sample collection and seawater pH; *solid triangles* down-core samples; *open triangles* surface samples; *solid stars* 'older stage'-filling of tubular concretion-old material / inside of samples / matrix; *open stars* 'younger stage'-walls of tubular concretion / surface of samples / cement; *solid square* bioturbation tube; *solid circle* dolostone at 97cmbsf

position of the precipitating fluid, and the pH. Since the carbonates formed near the sediment surface, the present in situ temperature corresponds to the equilibrium temperature at which precipitation occurred (see also Methods section). The $\delta^{18}O$ of the fluid in equilibrium with the individual carbonate mineral phases can be calculated using the following's experimental equations:

Equilibrium $\delta^{18}O$ of fluid precipitating aragonite (transformed from Grossman and Ku 1986):

$\delta^{18}O_{water}$ (SMOW) = $\delta^{18}O_{arag}$ (PDB) – (19.7– t)/4.34

Equilibrium $\delta^{18}O$ of fluid precipitating HMC (transformed from Friedman and O'Neil (1977):

$\delta^{18}O_{water}$ (SMOW) = exp[ln(1,000 + $\delta^{18}O_{HMC}$ (PDB) – (2780000/(273 + t)^2 –2.89 + 0.06 $MgCO_3$ (mol%)/1,000) –1,000)×1.03086 + 30.86

Equilibrium $\delta^{18}O$ of fluid precipitating LMC (transformed from Kim and O'Neil (1997):

$\delta^{18}O_{water}$ (SMOW) = exp[ln(1,000 + $\delta^{18}O_{LMC}$ (PDB) – (18030/(273 + t)–32.42)/1,000) –1,000]×1.03086 + 30.86

Equilibrium $\delta^{18}O$ of fluid precipitating proto-dolomite (transformed from Irwin (1980):

$\delta^{18}O_{water}$ (SMOW) = sqr[(5.55 – 0.34 $\delta^{18}O_{Proto}$ (PDB)/0.34)^2 – 31.9 – t – 5.55 $\delta^{18}O_{Proto}$ (PDB) + 0.17 $\delta^{18}O_{Proto}$ (PDB)/0.17] – 5.55 – 0.34 $\delta^{18}O_{Proto}$ (PDB)/0.34

A new complexity arises from the recently established pH-effect on the O-isotope fractionation during carbonate precipitation introduced by Zeebe (2001). The author shows that for 1 pH unit lower, the $\delta^{18}O$ of the carbonate is 1.42‰ "heavier". If the pH of the precipitating fluid is at most about 0.1–0.2 pH units lower than that of bottom water, then there is an increase in the equilibrium $\delta^{18}O_{water}$ up to 0.5‰ PDB, which falls within the uncertainty range of the approach used here. Figure 8 summarizes the $\delta^{18}O$ equilibrium calculations and shows that most of the carbonates have equilibrated with fluids with $\delta^{18}O$ more enriched than today's ocean water. The most extreme ^{18}O-enrichment is in the fillings of tubular concretions and a bioturbation tube. The bioturbation tube concretion has equilibrated $\delta^{18}O_{water}$ as high as +4.6, indicating that they may have precipitated from clay dehydration water. As shown by Hensen et al. (2004), there is clay dehydration water vented at the flank of Mound #11 with a $\delta^{18}O$ composition as high as +4.72‰ SMOW. A number of newly precipitated carbonates, for example, the cement of chemoherm carbonates and seepage-associated carbonates, have δ ^{18}O in a range of between glacial ocean water and today's ocean water; i.e., 0 to +1.0‰ SMOW. This indicates that they have been equilibrated with bottom seawater. Most of the samples appear to have equilibrium $\delta^{18}O$ values in the range of 1 to 3.5‰ SMOW, probably precipitated from mixtures of gas-hydrate water, clay dehydration water and bottom seawater.

The gas hydrate-associated carbonates from Mound #11 probably precipitated from fluids containing a component of hydrate water. The available pore water data from three gas-hydrate cores of Mound #11 (M54/ TVMUC138, M54/GC 109, M54/GC143) suggest a first order estimate involving fluid sources. The $\delta^{18}O_{water}$ of pore water at depth in core M54/GC109 at 185 cmbsf is 1.36‰ SMOW whereas the gas hydrate water itself at 216–242 cmbsf is +4.03±0.09‰ SMOW (Hensen et al. 2004). The established fractionation between hydrate water and 0‰ SMOW seawater is 3.0±0.1‰ SMOW (Suess et al. 1999), here hydrate formation shows further fractionation of the clay-dehydration water. The precipitating fluid is calculated at 3.5‰ SMOW, containing 78‰ hydrate water and 22‰ pore water. The other case (M54/ TVMUC138) shows the $\delta^{18}O_{water}$ of pore water at 2.78‰ between 0–1 cmbsf, and the corresponding carbonate sample—a chimney piece from the surface—

shows a fluid composition for two successive generations of aragonite to be 2.5 and 1.5‰ SMOW suggesting that the chimney formed from recent seawater (Fig. 2E).

The evolution of fluid venting

The mineralogical information, the stable isotope data and results of the fabric analysis from the authigenic carbonates also provide information on how the fluid may have evolved. The fabric indicates that pure aragonite filling the fractures and cavities in chemoherm and gas hydrate-associated carbonates formed later than the matrix cement. Fillings of tubular concretion also formed later than the host wall. Calculating the isotopic composition of these precipitating stages, shows the change in the $\delta^{18}O$ of pore water. Figure 8 shows that the equilibrium $\delta^{18}O$ of the precipitating fluid of 'older stage' are more enriched than those of 'younger stage'. Figure 9 shows the equilibrium $\delta^{18}O$ of the precipitating fluid for aragonite samples only, the data trend shows that the precipitating fluid is getting more depleted with time with respect to $\delta^{18}O$. The reason is that formation of authigenic carbonates reduces the permeability enough so that as the flow of deep fluids is weakened, more pore water or even seawater from the surrounding environment becomes involved during the later precipitation stages.

There is further evidence that the O-isotope evolution of fluid changed through time and was recorded by the authigenic carbonates. The mineralogy and $\delta^{18}O$ values from a set of concretions obtained downcore at Mound #10 reflect such an evolution. The concretions originally may have formed near the seafloor via AOM in the zone of sulfate reduction and later became buried. In this case, the pH and temperature of the precipitating fluid could have been constant through time and the change in calculated $\delta^{18}O$ of the precipitating fluid could be real. Figure 10 shows that the calculated fluid composition gradually changed from +2.8‰ SMOW at 315 cmbsf to 1.5‰ SMOW at 30 cmbsf. At the same time the calcite mineralogy changed from 2.1 mol% $MgCO_3$ to 6.8 mol% $MgCO_3$. Assuming that the deeper concretions formed earlier than the shallower ones and that the initially precipitated HMC had a higher $MgCO_3$ content, LMC at depth result from phase transformation with time because of metastable HMC. Such a change in the $\delta^{18}O$ of the precipitating fluid would be in agreement with a decrease in flow intensity or stronger dilution.

The C-isotope distribution provides similar evidence for an evolution of fluid. The most highly ^{13}C-depleted carbonates are the "chemoherm and seepage" carbonates, next are the "older" concretions followed by the "younger" concretions. Hereby criteria for differentiating are based on fabric, e.g., 'open tubes', 'wall' or "filling" as a progression with time. This implies a qualitative change in venting activity as follows: (1) the most intense venting rapidly advects methane-charged fluid through the seafloor, forming chemoherm and seepage carbonates; (2) less intense venting has advection rates not quite strong enough to reach the seafloor but rather form carbonate-cemented channel walls; (3) the least intense and youngest event clearly is caused by a weakened flow of methane-charged fluids cementing the fillings of tubes. A change in ^{13}C-depleted authigenic carbonates is to be expected, corroborating the interpretation of O-isotope changes.

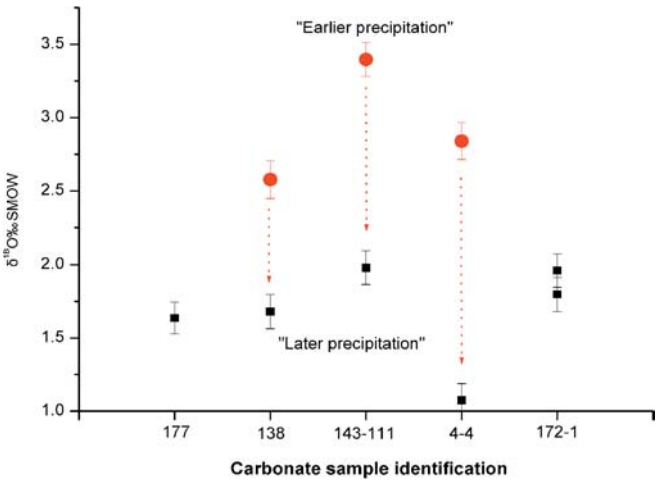

Fig. 9 Calculated equilibrium composition of precipitating fluid for different generations of aragonites at current bottom water temperatures ±0.5 °C. *Solid circles* Matrix of gas hydrate or chemoherm carbonates. *Solid squares* Aragonite cement

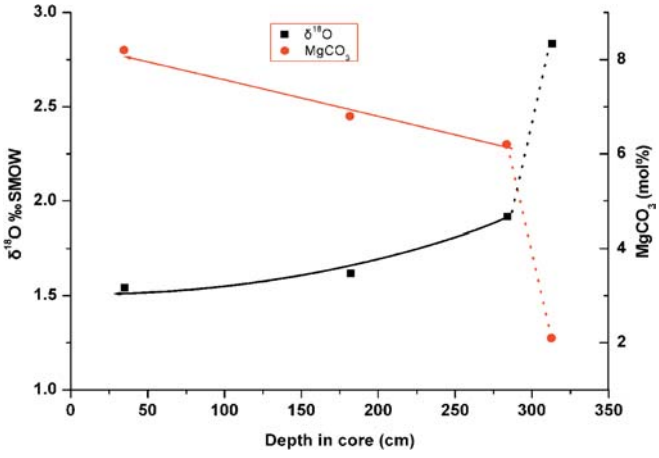

Fig. 10 Calculated equilibrium composition of precipitating fluids for calcareous concretions at four down-core depths from Station M54/143, the current bottom water temperature and pH are assumed to be the same at the time when the concretions were formed. Note systematic down-core change in MgCO3 content and the calculated equilibrium fluid $\delta^{18}O$

Dolomitic concretions: Insight into subsurface processes

Dolostones were observed and sampled at the plateau above Jaco Scarp and Mound #11. There are several lines of evidence favor the view that these dolostones formed in the subsurface and became exhumed by tectonic processes. In contrast to the authigenic carbonates, the large

spread of $\delta^{13}C$ between −11.1 and −44.2‰ PDB, but reasonably well constrained $\delta^{18}O$ between +5.7 and +8.1‰ PDB, indicate a geochemical setting where anaerobic methane oxidation is influenced by the addition of isotopically enriched carbon. This scenario is known to occur at depth (Claypool and Kaplan 1974), and evidence is provided by the DIC-values shown in Table 4. Greinert et al. (2001) showed with a much larger isotope data set from dolostones of the Cascadia margin that large C-isotopic variations are the result of depleted-C derived from anaerobic oxidation of methane mixed with enriched-C derived from methanogenesis. Among the samples from Cascadia margin there were dolostones with $\delta^{13}C$ values >+10‰ and up to +24‰ PDB. The strongly depleted C-isotope values encountered at the Costa Rica margin suggest a significant input of oxidized methane. This implies that the primary authigenic carbonate formed within the sulfate reduction zone. Depending on the advection rate of methane-rich fluids, this zone can be a few millimeters to tens of meters thick. Thus, a primary carbonate phase (HMC?) formed within the first meters of the sediment column, which by subsequent burial was transformed to dolostones with septarian cracks. The origin of the cracks is speculative; they could be the result of excess pore pressure (Hounslow 1997) or could result from volume shrinkage due to phase transition from HMC to dolomite.

Enigmatic lithic clasts: Implication for source depth of extruded material

Subduction and compaction of the sediment load not only lead to the regional expulsion of fluids from the downgoing sediments, but also channel deep lithic material to the surface through the extensional faulting system characteristic for the subduction erosion of the Costa Rica margin (Moerz et al, in press). Evidence for deep-sourced lithic material cemented by carbonate was found in tubular concretions from Mound Quepos (SO163/TVG9-5, SO163/TVG8-1), chemoherm carbonates from Mound 12 (SO163/TVG4-4) and a gas hydrate-associated concretion from Mound #11 (M54/GC143–111). The fabric of the walls of tubular concretions is very different from that of the fillings. The fillings usually are cemented by LMC and contain abundant angular clay clasts, quartz and glauconite grains. There are also later-stage diagenetic changes including dissolution, recrystallization and replacement (Fig. 4D, E). This suggests that the material of fillings may have been channeled from deep strata. Sample GC143–111 (Fig. 4C) at Mound #11 and clasts of sample TVG4–4 (Fig. 4A) show similar features. Since the glauconite is usually formed in shallow water, we hypothesize that the material of the filling originated from the base of the upper plate before it subsided from subduction erosion.

Conclusions

Authigenic carbonates are good candidates for providing a long-term record of changing processes at fluid expulsion sites. Mineralogical, petrographic and isotopic analyses of various types and shapes of the carbonates off the Costa Rica margin reveal that methane-rich fluids played a role as the source of carbon in their formation: gas hydrate carbonates are form from thermogenic methane, chemoherm and seepage-associated crusts from biogenic methane. The intermediate C-isotope values of the other carbonate concretions probably reflect an origin from the biogenic methane with addition of "enriched" C-isotopes from pore water DIC. The $\delta^{18}O$ compositions of precipitating fluid are enriched with respect to 0‰ SMOW with three possible fluid sources: clay dehydration water, hydrate water, and seawater. Fillings of chimney-like concretion are precipitated from clay-dehydration water; the $\delta^{18}O$ of the precipitating fluids of seepage-associated crusts and chemoherms are equilibrated with bottom water. The other carbonate types may have been precipitated from mixtures of clay-dehydration water, gas hydrate water and seawater. The gas hydrate-associated carbonates probably contain a significant portion of gas hydrate water. The formation of carbonate reduces the permeability of the sediments and hence weakens the advection of deep-fluid flow, therefore more seawater participates in carbonate formation, this results in the $\delta^{18}O$ of carbonate becoming depleted with time. The exotic glauconite sandstone clasts found in the fillings of tubular calcareous concretions indicate that they came from the deep strata which originally formed in shallow water and later subsided due to subduction erosion. Our data demonstrate that the different carbonates types could be related to source depth and fate of the ascending methane-bearing fluids and hence can be used to reconstruct the dewatering and fluid-venting history of the forearc area off northern Costa Rica and southern Nicaragua.

Acknowledgments We thank the R/V SONNE 163 and R/V METEOR 54 crew and the shipboard scientific parties for their cooperation and help at sea. We also thank Christian Hensen and Susan Mau for providing unpublished data, Ralf Tiedemann for C- and O- isotope analyses, and Jutta Heinze for assistance with XRD analysis. Additional thanks go to Jens Greinert for constructive discussion, to two anonymous reviewers and to Gerhard Bohrmann (RCOM, Bremen) for helpful comments and suggestions and to Zona Suess for help with the English. This study was funded by SFB 574 and partially supported by the National Major Fundamental Research and Development Project of China (973 project, No. G20000467–03). This is SFB contribution Nr. 50.

References

Aharon P (1994) Geology and biology of modern and ancient submarine hydrocarbon seeps and vents: an introduction. Geo-Mar Lett 14:69–73

Boetius A, Ravenschlag K, Schubert CJ, Rickert D, Widdel F, Gieseke A, Amann R, Jorgensen BB, Witte U, Pfannkuche O (2000) A marine microbial consortium apparently mediating anaerobic oxidation of methane. Nature 407:623–626

Bohrmann G, Greinert J, Suess E, Torres M (1998) Authigenic carbonates from the Cascadia subduction zone and their relation to gas hydrate stability. Geology 26(7):647–650

Bohrmann G, Heeschen K, Jung C, Weinrebe W, Baranov B, Cailleau B, Heath R, Hühnerbach V, Hort M, Mason D (2002a) Widespread fluid expulsion along the seafloor of the Costa Rica convergent margin. Terra Nova 14(2):69–79

Bohrmann G, Suess E, Greinert J, Teichert B, Naehr T (2002b) Gas hydrate carbonates from Hydrate Ridge, Cascadia margin: indicators for near-seafloor clathrates. Proc 4th Intl Gas Hydrate Research Conf, Yokohama, pp 102–107

Borowski WS, Paull CK, Ussler W III (1999) Global and local variations of interstitial sulfate gradients in deep-water, continental margin sediments: sensitivity to underlying methane and gas hydrates. Mar Geol 159:131–154

Claypool GE, Kaplan IR (1974) The origin and distribution of methane in marine sediments. In: Kaplan IR (ed) Natural gases in marine sediments. Plenum, New York, pp 99–139

Friedman I, O'Neil JR (1977) Compilation of stable isotope fractionation factors of geochemical interest. In: Fleischer M (ed) Data of geochemistry. US Geol Surv Prof Pap 440-KK, 6th edn, Reston, VA

Goldsmith JR, Graf DL, Heard HC (1961) Lattice constants of the calcium-magnesium carbonates. Am Mineral 46:453–457

Greinert J, Bohrmann G, Suess E (2001) Gas hydrate-associated carbonates and methane-venting at Hydrate Ridge: classification, distribution and origin of authigenic lithologies. In: Paull CK, Dillon WP (eds) Natural gas hydrates: occurrence, distribution and detection. Geophys Monogr, Am Geophys Union, Washington, DC, pp 99–113

Grevemeyer I, Kopf AJ, Kaul N, Heesemann M, Gennerich H-H, Wallmann K, Weinrebe W (2004) Fluid flow through active mud dome Mound Culebra offshore Nicoya Peninsula, Costa Rica: evidence from heat flow surveying. Tectonophysics (in press)

Grossman EL, Ku TL (1986) Oxygen and carbon isotope fractionation in biogenic aragonite: temperature effects. Chem Geol 59:59–74

Hensen C, Wallmann K, Schmidt M, Ranero C, Sahling H, Suess E (2004) Fluid expulsion related to mud volcanism at Costa Rica continental margin-a window to the subducting slab. Geology 32(2):201–204

Hey R (1977) Tectonic evolution of the Cocos-Nazca spreading center. GSA Bull 88:1404–1420

Hounslow MW (1997) Significance of localized pore pressures to the genesis of septarian concretions. Sedimentology 44:1133–1147

Irwin H (1980) Early diagenetic precipitation and pore fluid migration in the Kimmeridge Clay of Dorset, England. Sedimentology 27:577–591

Kim S-T, O'Neil JR (1997) Equilibrium and non-equilibrium oxygen isotope effects in synthetic carbonates. Geochim Cosmochim Acta 61:3461–3475

Kimura G, Silver E, Blum P (1997) Proceedings of the Ocean Drilling Program, Leg 170 Scientific Party, Initial Reports 170. Ocean Drilling Program, College Station, TX

Kulm LD, Suess E (1990) Relationship between carbonate deposits and fluid venting: Oregon accretionary prism. J Geophys Res 95:8899–8915

Kulm LD, Suess E, Moore JC, Carson B, Lewis BT, Ritger SD, Kadko DC, Thornburg TM, Embley RW, Rugh WD, Massoth GJ, Langseth MG, Cochrane GR, Scamman RL (1986) Oregon subduction zone: venting, fauna and carbonates. Science 231:561–566

Le Pichon X, Henry P, Lallemant S (1993) Accretion and erosion in subduction zones: the role of fluids. Annu Rev Earth Planet Sci 21:307–331

Luff R, Wallmann K (2003) Fluid flow, methane fluxes, carbonate precipitation and biogeochemical turnover in gas hydrate-bearing sediments at Hydrate Ridge, Cascadia Margin: numerical modeling and mass balances. Geochim Cosmochim Acta 67(18):3403–3412

Lumsden DS (1979) Discrepancy between thin-section and x-ray estimates of dolomite in limestone. J Sediment Petrol 49:429–436

Milliman J (1977) Role of calcareous algae in Atlantic continental margin sedimentation. In: Fluegel E (ed) Fossil algae. Springer, Berlin Heidelberg New York, pp 232–247

Mörz T, Fekete N, Kopf A, Brückmann W, Kreiter S, Huehnerbach V, Masson D, Hepp DA, Schmidt M, Kutterolf S, Sahling H, Abegg F, Spiess V, Suess E, Ranero CR (2004) Styles and productivity of mud diapirism along the Middle American Margin / Part 2: Mound Culebra and Mounds 11 and 12. Nato Science Series, Kluwer Academic Publishers, Dordrecht (in press)

Mörz T, Kopf A, Brueckmann W, Fekete N, Huenerbach V, Masson D, Hepp DA, Suess E, Weinrebe W (2004) Styles and productivity of mud diapirism along the Middle American Margin, Part 1: Margin evolution, segmentation, dewatering and mud diapirism. Nato Science Series, Kluwer Academic Publishers, Dordrecht (in press)

O'Hara SCM, Dando PR, Schuster U, Bennis A, Boyle JD, Chui FTW, Hatherell TVJ, Niven SJ, Taylor LJ (1995) Gas seep induced interstitial water circulation: observations and environmental implications. Cont Shelf Res 15(8):931–948

Paull CK, Chanton J, Neumann AC, Coston JA, Martens CS, Showers W (1992) Indicators of methane-derived carbonates and chemosynthetic organic carbon deposits: examples from the Florida Escarpment. Palaios 7:361–375

Pecher IA, Kukowski N, Ranero CR, Von Huene R (2001) Gas hydrates along the Peru and Middle America Trench Systems. In: Natural gas hydrates: occurrence, distribution, and detection. Am Geophys Union 124:257–271

Peckmann J, Reimer A, Luth U, Luth C, Hansen BT, Heinicke C, Hoefs J, Reitner J (2001) Methane-derived carbonates and authigenic pyrite from the northwestern Black Sea. Mar Geol 177(1–2):129–150

Ranero CR, Phipps Morgan J, McIntosh K, Reichert C (2003) Bending-related faulting and mantle serpentinization at the Middle America Trench, Nature, 425:367–373

Ranero CR, von Huene R (2000) Subduction erosion along the Middle America convergent margin. Nature 404: 748–752

Ritger S, Carson B, Suess E (1987) Methane-derived authigenic carbonates formed by subduction-induced pore-water expulsion along the Oregon/Washington margin. GSA Bull 98:147–156

Roberts HH, Aharon P (1994) Hydrocarbon-derived carbonate buildups of the northern Gulf of Mexico continental slope: a review of submersible investigation. Geo-Mar Lett 14:135–148

Saito S, Goldberg D (2001) Compaction and dewatering processes of the oceanic sediments in the Costa Rica and Barbados subduction zones: estimates from in situ physical property measurements. Earth Planet Sci Lett 191:283–93

Soeding E, Wallmann K, Suess E, Flueh ER (eds) (2003) Cruise report M54/2+3: fluids and subduction Costa Rica 2002, GEOMAR Report 111, 366 pp

Suess E (2002a) Gashydrat—Eine Verbindung aus Methan und Wasser. Nova Acta Leopoldina NF 85(323):123–146

Suess E (2002b) The evolution of an idea: from avoiding gas hydrates to actively drilling for them. In: achievements and opportunities of scientific ocean drilling. The legacy of the Ocean Drilling Program. JOIDES J, 28(1):45–50

Suess E, Bohrmann G, Rickert D, Kuhs WF, Torres M, Trehu A, Linke P (2002) Properties and fabric of near-surface methane hydrates at Hydrate Ridge, Cascadia margin. Proc 4th Int Gas Hydrate Research Conf, Yokohama, pp 740–744

Suess E, Carson B, Ritger S, Moore JC, Jones M, Kulm LD, Cochrane G (1985) Biological communities at vent sites along the subduction zones off Oregon. In: Jones ML (ed) The hydrothermal vents of the Eastern Pacific: an overview. Bull Biol Soc Wash 6:475–484

Suess E, Torres ME, Bohrmann G, Collier RW, Greinert J, Linke P, Rehder G, Tréhu A, Wallmann K, Winckler G, Zuleger E (1999) Gas hydrate destabilization: enhanced dewatering,

benthic material turnover and large methane plumes at the Cascadia convergent margin. Earth Planet Sci Lett 170:1–15

Torres ME, Wallmann K, Trehu AM, Bohrmann G, Borowski WS, Tomaru H (2003) Constraints on gas hydrate dynamics at Hydrate Ridge based on dissolved chloride data: I. Ridge summit. Earth Planet Sci Lett (submitted)

Vannucchi P, Scholl DW, Meschede M, McDougall-Reid K (2001) Tectonic erosion and consequent collapse of the Pacific margin of Costa Rica: combined implications from ODP Leg 170, seismic offshore data and regional geology of the Nicoya Peninsula. Tectonics 20:649–668

von Huene R, Lallemand S (1990) Tectonic erosion along the Japan and Peru convergent margins. Geol Soc Am Bull 102:704–720

von Huene R, Ranero CR (2003) Subduction erosion and basal friction along the sediment starved convergent margin off Antofagasta Chile. J Geophys Res 108:2079, DOI10.1029/2001JB001569

Warthmann R, van Lith Y, Vasconcelos C, McKenzie JA, Karpoff A-M (2000) Bacterially induced dolomite precipitation in anoxic culture experiments. Geology 28(12):1091–1094

Weinrebe W, Flüh E (eds) (2000) R.V. SONNE Cruise Report SO-163, SUBDUCTION I (March 13–April 20, 2002; Balboa—Balboa). GEOMAR Report 106, Kiel, 530 pp

Zeebe RE (2001) Seawater pH and isotopic paleotemperature of Cretaceous oceans. Palaeogeogr Palaeoclimatol Palaeoecol 170:49–57